X-ray microscopy of soft and hard human tissues

Bert Müller, Georg Schulz, Hans Deyhle, Anja K. Stalder, Bernd Ilgenstein, Margaret N. Holme, Timm Weitkamp , Felix Beckmann, and Simone E. Hieber

Citation: AIP Conference Proceedings **1696**, 020010 (2016); doi: 10.1063/1.4937504
View online: http://dx.doi.org/10.1063/1.4937504
View Table of Contents: http://scitation.aip.org/content/aip/proceeding/aipcp/1696?ver=pdfcov
Published by the AIP Publishing

X-Ray Microscopy of Soft and Hard Human Tissues

Bert Müller[1, a)], Georg Schulz[1, b)], Hans Deyhle[1, c)], Anja K. Stalder[1, d)], Bernd Ilgenstein[1, e)], Margaret N. Holme[1, f)], Timm Weitkamp[2, g)], Felix Beckmann[3, h)], and Simone E. Hieber[1, i)]

[1]*Biomaterials Science Center (BMC), University of Basel, c/o University Hospital, 4031 Basel, Switzerland*
[2]*Beamline ANATOMIX, Synchrotron Soleil, L'Orme des Merisiers, Saint Aubin - B.P. 48, 91192 Gif sur Yvette, France*
[3]*Institute of Materials Research, Helmholtz-Zentrum Geesthacht, Max-Planck-Str. 1, 21502 Geesthacht, c/o HZG at DESY, Notkestr. 85, 22607 Hamburg, Germany*

[a)]Corresponding author: bert.mueller@unibas.ch
[b)]georg.schulz@unibas.ch
[c)]hans.deyhle@unibas.ch
[d)]anja.stalder@unibas.ch
[e)]bernd.ilgenstein@unibas.ch
[f)]m.holme@imperial.ac.uk
[g)]weitkamp@synchrotron-soleil.fr
[h)]felix.beckmann@hzg.de
[i)]simone.hieber@unibas.ch

Abstract. The simultaneous *post mortem* visualization of soft and hard tissues using absorption-based CT remains a challenge. If the photon energy is optimized for the visualization of hard tissue, the surrounding soft tissue components are almost X-ray transparent. Therefore, the combination with other modalities such as phase-contrast CT, magnetic resonance microscopy, and histology is essential to detect the anatomical features. The combination of the 2D and 3D data sets using sophisticated segmentation and registration tools allows for conclusions about otherwise inaccessible anatomical features essential for improved patient treatments.

INTRODUCTION

The simultaneous visualization of soft and hard tissues by conventional CT remains a challenge. It is well known that, outside the absorption edges, X-ray absorbance is approximately inversely proportional to the third power of the photon energy [1]. Owing to the heterogeneity of the human tissues the best choice of the photon energy is difficult to identify. The hard tissue components or highly X-ray absorbing implants usually yield streak artifacts, see for example [2]. At the photon energy optimized for the hard tissue, the surrounding soft tissue components are almost X-ray transparent and therefore yield poor contrast. The choice of the photon energy for heterogeneous tissue using phase-contrast CT, rather than absorption contrast, is easier, as the real part of the refractive index varies much less with elemental composition than the absorbance [3]. Therefore, both absorption and phase-contrast imaging provide complementary information [4, 5]. Other techniques including magnetic resonance microscopy and histology are also complementary [6]. Recently, it has been demonstrated that the combination of images from different modalities applying sophisticated registration tools allows for conclusions about otherwise inaccessible anatomical features. The acquired knowledge is essential for improved patient treatments in fields such as neurodegenerative and cardiovascular diseases [7] as well as oral health [8]. The question arises to what extent the assessment developed for specific modality combinations selected for the heterogeneous tissue of interest can be applied for other combinations that may be better suited for different heterogeneous material or tissue.

XRM 2014
AIP Conf. Proc. 1696, 020010-1–020010-4; doi: 10.1063/1.4937504

MORPHOLOGY OF A DISEASED ARTERY

Atherosclerosis is a common cardiovascular disease, which is associated with inflammation, plaque formation and constriction of the affected vessels. For the decisions on the possible treatments of the diseased part of the plaque-containing artery the medical experts quantify the degree of constriction taking advantage of contrast media and CT. They have to assume that the maximal lumen perfused by the contrast agent corresponds to the healthy situation. Figure 1 demonstrates that this is not necessarily the case. The three-dimensional representation of the 7.5 mm-long part of the diseased human coronary artery originates from synchrotron radiation-based μCT in absorption contrast mode (HZG, DESY, Hamburg, Germany) [7]. The region available for blood flow and thus accessible by contrast agent is marked in yellow, while the total cross-section of the lumen is indicated in red. The cross-section of the non-obstructed artery varies from 5 % (arrowheads on the left) to 25 % (arrowheads on the right) with respect to the total lumen at the related position. As a consequence, the radiologist would consider a 75 % stenosis, whereas the vessel is constricted by 95 %.

The distribution of the average wall shear stress can be derived from flow simulations based on SRμCT data [7]. For this purpose, the lumen has not only to be extracted from the raw data (segmentation) but also converted to a mesh representation [7]. For the present diseased artery the average wall shear stress varies from approximately 5 Pa to values well above 13 Pa [7].

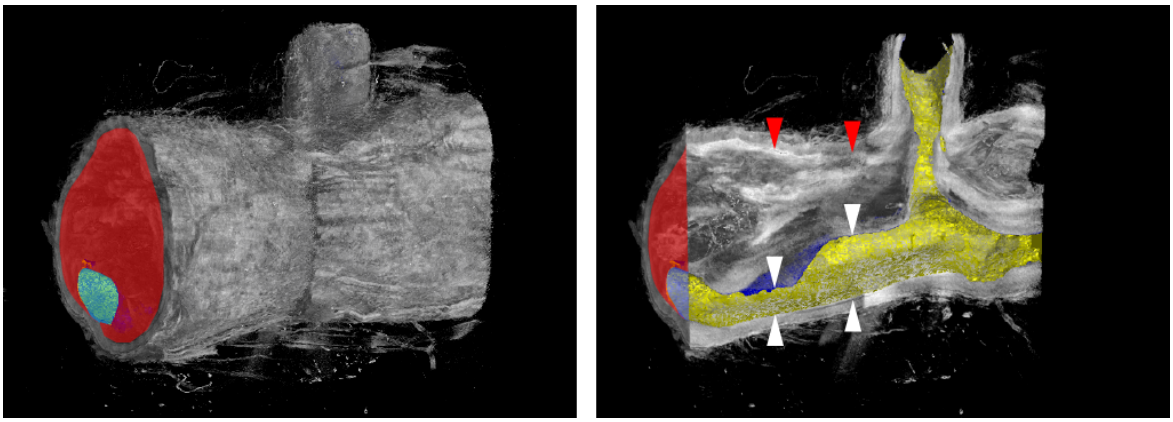

FIGURE 1. The morphology of the diseased human coronary artery shows modulations in the cross section giving rise to significant changes in the average wall shear stress along the blood flow. Please note that the diameter of the lumen given in blue is much smaller than the original vessel diameter indicated by the red-colored cross section.

SEGMENTING THE ANATOMICAL FEATURES OF HUMAN CEREBELLUM

A selected slice through the human cerebellum, as displayed in Fig. 2, illustrates the power and complementary nature of grating-based μCT and MR microscopy [6]. Whereas grating-based phase μCT (a) performed at beamline ID19 of the European Synchrotron Radiation Facility (ESRF, Grenoble, France) shows a high contrast between white matter (1) and *stratum granulosum* (2) and between *stratum moleculare* (3) and *stratum granulosum* (2) there is almost no contrast between white matter (1) and *stratum moleculare* (3). On the contrary, MR microscopy data (b), acquired with a 9.4 T small animal scanner (Bruker BioSpec, Bruker BioSpin MRI, Ettlingen, Germany), shows superb contrast between white (1) and gray matter (2+3) but almost no contrast between *stratum granulosum* (2) and *stratum moleculare* (3).

The slices of the registered three-dimensional datasets [9] can be fused using the red and blue channels of the RGB representation. This method directly visualizes the contributions from the two imaging techniques in a semi-quantitative manner and permits the distinction of otherwise indistinguishable anatomical features, i.e. white matter (dark red color, i.e. strong CT and weak MR signal), *stratum granulosum* (violet color, i.e. strong signals from CT and MR), and *stratum moleculare* (blue color, weak signal from CT and strong signal from MR).

One can also combine the three-dimensional MR and CT data with subsequently prepared histology slices from the same brain tissue and identify even more anatomical features, which include the blood vessels of sizes down to the capillary level [6].

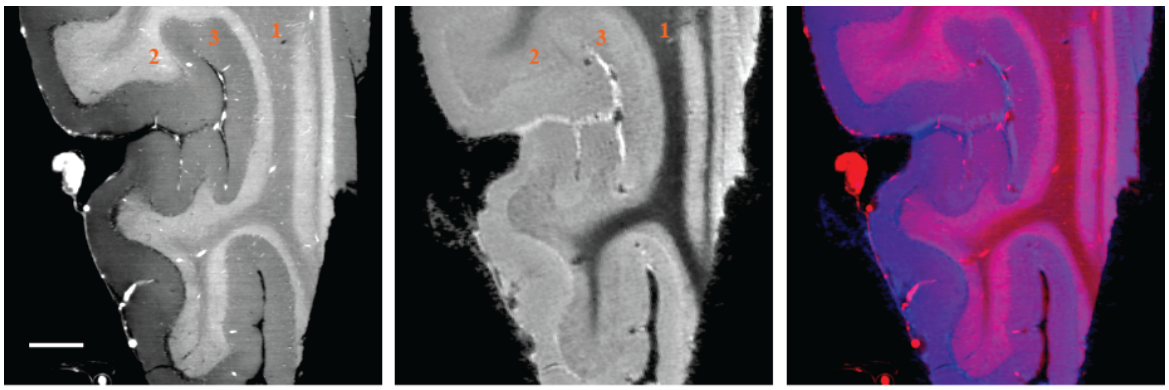

FIGURE 2. Representative slice of the cerebellum imaged using (a) grating-based phase CT and (b) MR microscopy. The color image given in (c) is a superposition of the phase CT image (a, red channel) and the MR microscopy image (b, blue channel).

BONE AUGMENTATION

Bone grafting substitutes instead of harvested autologous bone play an increasingly important role in augmenting bone for sufficient bone offer before the insertion of dental implants. In the present study, a vertical bone defect was augmented using BoneCeramic® (Institute Straumann AG, Basel, Switzerland) [8,11]. The specimen was taken after a four-month bone healing at the position of the future implant and was scanned using the µCT-setup at the beamline W2 (HZG/DESY, Hamburg, Germany) [8]. Subsequent to the non-destructive CT evaluation, several histological slices were prepared. It is demanding to register these artifact-containing, two-dimensional histology slices with the less detailed three-dimensional tomography data [10]. After the slice from histology is manually and/or automatically aligned to the tomography data, the mapping can be exploited to obtain a joint histogram (see Fig. 3(e)).

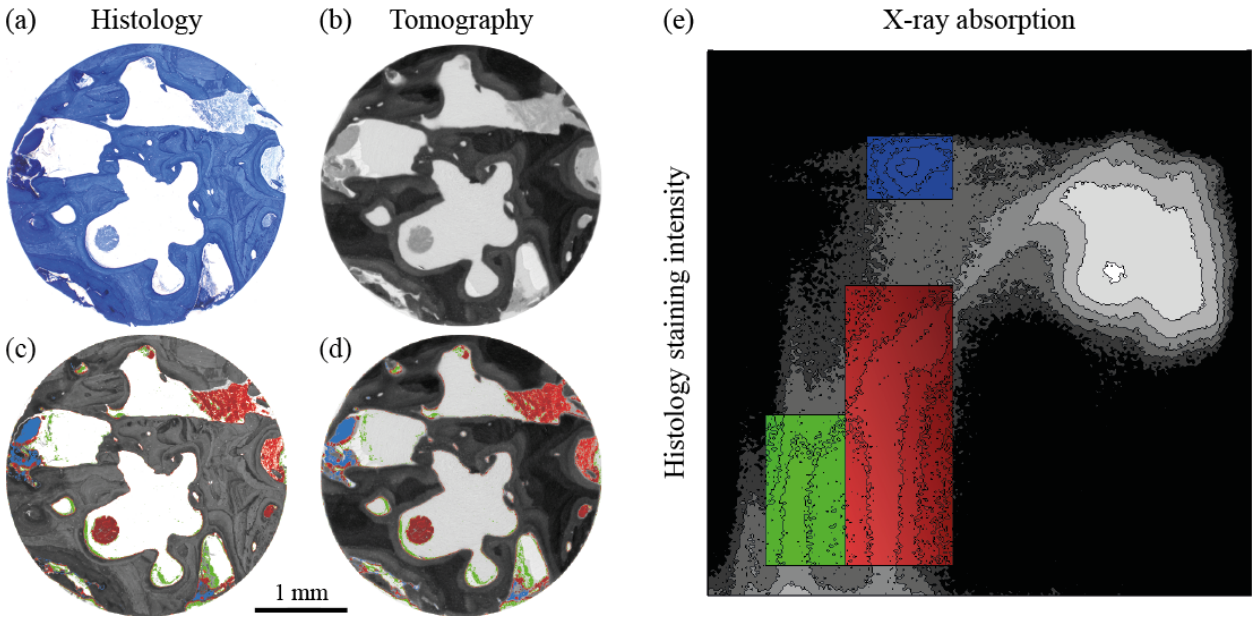

FIGURE 3. The generation of a meaningful joint histogram requires the precise manual or automatic mapping of the histology slice (a) within the CT data (b). The joint histogram shows the frequency of the occurring combinations between the staining intensity from the histological sections and the local X-ray absorption of the µCT measurements (e). It can be used to select color-coded anatomical features within the registered, gray-scale histology (c) and the related tomography slice (d).

Such a histogram of histology and tomography slices allows for the segmentation of the partially degraded augmentation material (red color), the early-formed bone (blue color) and the soft tissue (granulation matrix)/mineralizing bone matrix (green color). The gradient from dark to bright red color represents the degradation of the augmentation material. The identified features cannot be recognized by histology or µCT alone. Using only µCT the red- and blue-colored features, i.e. partially resorbed augmentation material and newly formed bone are located at the same X-ray absorption values and cannot be separated. Using only histology the green- and red-colored features cannot be separated based on their staining intensity. Therefore the partially disintegrated bone augmentation material cannot be segmented from histology and tomography alone, but with the appropriate combination and the support of two- to three-dimensional registration and the joint histogram analysis, the location of BoneCeramic® is clearly detected.

CONCLUSIONS

The non-destructive tomography measurements in X-ray absorption and phase-contrast modes can be combined with the application of established histology and MR-microscopy techniques via sophisticated data evaluation methods. The combination gives rise to the thorough three-dimensional characterization of soft and hard human tissues. The ongoing projects focus on the micro- and nano-anatomy of a variety of healthy and diseased tissues in a standardized and quantitative manner.

ACKNOWLEDGMENTS

The authors thank C. Waschkies and M. Rudin (ETH Zürich) for their support acquiring the MR microscopy data. The Swiss National Science Foundation financially supported the research activities by the following grants: *NO-Stress, a specific coronary vasodilator – nano-container for tailored NO release* within the National Research Program NRP62 "Smart Materials", *Micro- and nanoanatomy of human brain tissues* # CR23I2_147172, and *Multi-modal matching of two-dimensional images with three-dimensional data in the field of biomedical engineering* # 205321_150164. The French *Agence nationale de la recherche* (ANR) is acknowledged for support via EQUIPEX grant ANR-11-EQPX-0031 (project NanoimagesX).

REFERENCES

1. S. R. Stock, *Micro Computed Tomography: Methodology and Applications*. (CRC Press, 2008).
2. M. Luckow, H. Deyhle, F. Beckmann, D. Dagassan-Berndt and B. Müller, Eur. J. Radiol. **80**, e389-e393 (2011).
3. U. Bonse and F. Busch, Prog. Biophys. Mol. Bio. **65** (1-2), 133-169 (1996).
4. G. Schulz, T. Weitkamp, I. Zanette, F. Pfeiffer, F. Beckmann, C. David, S. Rutishauser, E. Reznikova and B. Müller, J. Roy. Soc. Interface **7** (53), 1665-1676 (2010).
5. M. Buscema, M. N. Holme, H. Deyhle, G. Schulz, R. Schmitz, P. Thalmann, S. E. Hieber, N. Chicherova, P. C. Cattin, F. Beckmann, J. Herzen, T. Weitkamp, T. Saxer and B. Müller, Proc. of SPIE **9212**, 921203 (2014).
6. G. Schulz, C. Waschkies, F. Pfeiffer, I. Zanette, T. Weitkamp, C. David and B. Müller, Sci. Rep. **2**, 826 (2012).
7. M. N. Holme, G. Schulz, H. Deyhle, T. Weitkamp, F. Beckmann, J. A. Lobrinus, F. Rikhtegar, V. Kurtcuoglu, I. Zanette, T. Saxer and B. Müller, Nat. Protocols **9** (6), 1401-1415 (2014).
8. A. Stalder, B. Ilgenstein, N. Chicerova, H. Deyhle, F. Beckmann, B. Müller and S. E. Hieber, Int. J. Mater. Res. **105** (7), 679-691 (2014).
9. B. Müller, H. Deyhle, S. Lang, G. Schulz, T. Bormann, F. Fierz and S. Hieber, Int. J. Mater. Res. **103** (2), 242-249 (2012).
10. N. Chicherova, K. Fundana, B. Müller and P. C. Cattin, Lecture Notes in Comp. Sci. **8673**, 243-250 (2014).
11. B. Ilgenstein, H. Deyhle, C. Jaquiéry, C. Kunz, A. Stalder, S. Stübinger, G. Jundt, F. Beckmann, B. Müller, S. E. Hieber, Proc. of SPIE **8506**, 85060M (2012).